Benzyl Alcohol and Block Copolymer Micellar Lithography: A Versatile Route to Assembling Gold and *in Situ* Generated Titania Nanoparticles into Uniform Binary Nanoarrays

Julien Polleux,[†,‡,*] Matthias Rasp,[†] Ilia Louban,[‡,§] Nicole Plath,[‡,§] Armin Feldhoff,[⊥] and Joachim P. Spatz[‡,§]

[†]Department of Molecular Medicine, Max Planck Institute of Biochemistry, 82152 Martinsried, Germany, [‡]Department of New Materials and Biosystems, Max Planck Institute for Intelligent Systems, 70569 Stuttgart, Germany, [§]Institute for Physical Chemistry, Biophysical Chemistry, University of Heidelberg, INF 253, 69120 Heidelberg, Germany, and [⊥]Institute of Physical Chemistry and Electrochemistry, Leibniz University Hannover, 30167 Hannover, Germany

ABSTRACT Simultaneous synthesis and assembly of nanoparticles that exhibit unique physicochemical properties are critically important for designing new functional devices at the macroscopic scale. In the present study, we report a simple version of block copolymer micellar lithography (BCML) to synthesize gold and titanium dioxide (TiO_2) nanoarrays by using benzyl alcohol (BnOH) as a solvent. In contrast to toluene, BnOH can lead to the formation of various gold nanopatterns *via* salt-induced micellization of polystyrene-*block*-poly(vinylpyridine) (PS-*b*-P2VP). In the case of titania, the use of BCML with a nonaqueous sol–gel method, the "benzyl alcohol route", enables the fabrication of nanopatterns made of quasi-hexagonally organized particles or parallel wires upon aging a ($BnOH-TiCl_4-PS_{846}$-*b*-$P2VP_{171}$)-containing solution for four weeks to grow TiO_2 building blocks *in situ*. This approach was found to depend mainly on the relative lengths of the polymer blocks, which allows nanoparticle-induced micellization and self-assembly during solvent evaporation. Moreover, this versatile route enables the design of uniform and quasi-ordered gold–TiO_2 binary nanoarrays with a precise particle density due to the absence of graphoepitaxy during the deposition of TiO_2 onto gold nanopatterns.

KEYWORDS: nonaqueous sol–gel process · block copolymer micellar lithography · *in situ* growth of nanoparticles · directed self-assembly · binary nanoarrays

Synthesis and assembly of nanoparticles that exhibit unique physicochemical properties[1–5] are critically important for the design of new functional devices at the macroscopic scale. Generally, bottom-up approaches prove to be effective in fabricating hierarchically nanostructured inorganic materials[6–8] and thin films[9–11] by controlling the nanoparticle shape, size, and surface chemistry.[6,7] Among the various synthetic methods such as surfactant-assisted routes[9] and advanced lithographic techniques,[12] block-copolymer micellar lithography (BCML) has been recognized as a facile and versatile approach for generating a wide variety of periodic nanostructures with sub-45 nm resolution and long-range order.[13–16] Amphiphilic diblock copolymers (dBCPs) undergo microphase segregation in solvents selective for one of the two blocks, resulting in the formation of various supramolecular structures.[17] For instance, upon transferring and organizing these structures *via* evaporation-induced self-assembly (EISA),[18] ordered micellar monolayers can be used as etching masks to structure the topography of coated wafers[19,20] and as templates for the fabrication of inorganic nanopatterns by using molecular precursors[21–23] or presynthesized nanoparticles.[24–26] In contrast to metals and transition metals,[22,27] the preparation of crystalline transition metal oxide nanoarrays is not well established despite their technological relevance.[21,28] Therefore, new strategies applicable to this class of materials are needed to further engineer a larger variety of functional nanostructured surfaces.

Titanium dioxide (TiO_2) is a well-characterized metal oxide system that exhibits interesting physicochemical properties and uses such as photocatalysis,[29] gas sensing,[30,31] photovoltaics,[32,33] lithium ion batteries,[34] and supercapacitors.[35] As crystallinity, size, and morphology dictate the performance of TiO_2 nanoparticles, it is also critical to control their organization for generating functional interfaces.[35–37] Although TiO_2 nanoarrays were reported by combining BCML with sol–gel processes[38–41] and chemical vapor deposition,[42] these approaches lead to the formation of nanopatterns that are poorly ordered or inhomogeneously distributed over extended areas due to limited control over template organization and titanium loading.

* Address correspondence to polleux@biochem.mpg.de.

Received for review April 21, 2011 and accepted July 20, 2011.

Published online July 20, 2011
10.1021/nn201470f

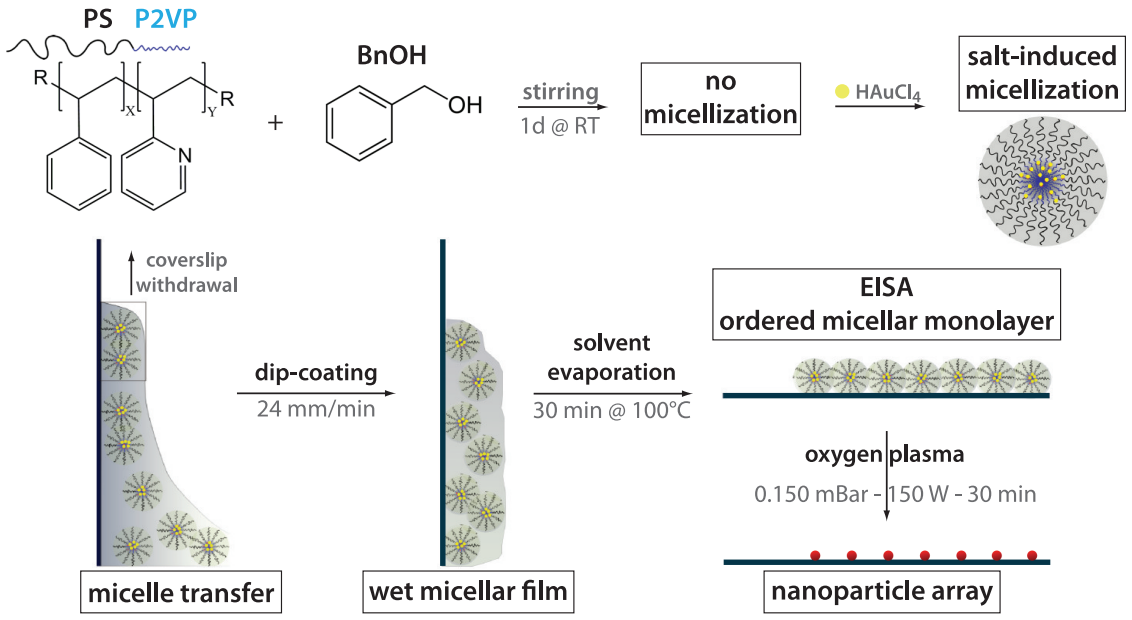

Scheme 1. Schematics describing the different experimental steps necessary for the preparation of gold nanoarrays *via* BnOH-assisted micellar lithography.

As a general alternative to replace the use of inorganic molecular precursors and intramicellar reactions, the placement of presynthesized nanoparticles within dispersed micelles[43] or onto self-assembled micellar monolayers[26,44,45] represents an elegant approach for synthesizing nanostructured surfaces. However, this method does not offer a reliable way for producing well-organized nanopatterns due to the difficulties in incorporating nanoparticles and their diffuse distribution in segregated nanodomains.

In the present study, we report a straightforward BCML approach applicable to gold and titanium dioxide. Instead of using aqueous sol–gel processes or presynthesized nanoparticles, the use of benzyl alcohol with BCML provides an effective approach for fabricating gold and TiO_2 nanoarrays of various morphologies by using $HAuCl_4$ and *in situ* generated TiO_2 nanoparticles as inorganic precursors. Moreover, this versatile route enables the design of gold–TiO_2 binary nanoarrays, which are heterogeneous in composition and morphology.

RESULTS AND DISCUSSION

Benzyl Alcohol As Alternative Solvent for Diblock Copolymer Micellar Lithography. Polystyrene-*block*-poly(vinylpyridine) (PS_x-*b*-$P2VP_y$ where *x* and *y* represent the number of monomer units) is commonly used in BCML to synthesize noble and transition metal nanoarrays. Consisting of an apolar PS block covalently linked to a polar P2VP domain, the solubilization of PS_x-*b*-$P2VP_y$ in toluene leads to the spontaneous formation of monodisperse reverse micelles, which are used as nanocarriers for inorganic precursors under acidic conditions. In the case of hydrogen tetrachloroaurate(III) trihydrate, the uptake of hydrochloric acid into the micelles results in the protonation of the P2VP core and the binding of $[AuCl_4]^-$. Moreover, the incorporation of such inorganic precursors makes the amphiphilic dBCP more hydrophilic, which further promotes micelle formation. The loaded micelles can then be used as templates to structure surfaces upon EISA and plasma treatment.[27]

With a chemical structure similar to toluene, benzyl alcohol (BnOH) is a convenient solvent due to its amphiphilic character, low vapor pressure, and low toxicity. The first use of BnOH to synthesize bulk nanohybrid materials was made using dBCP lamellar microdomains containing palladium (Pd) nanoparticles.[46] In that work, BnOH served two roles; it acted as a solvent to induce microphase segregation in highly concentrated dBCP solutions and as a reducing agent to convert Pd(II) ions to Pd(0) during solvent evaporation at 140 °C. Interestingly, this approach has never been adapted for lithographic techniques.

We set out to test the feasibility of BnOH as a potential solvent for BCML and to compare it with toluene. Both solvents were used to prepare gold-loaded micellar solutions upon dissolving PS_{1056}-*b*-$P2VP_{495}$ and $HAuCl_4$. With a boiling point of 204 °C, BnOH evaporates slowly at room temperature upon dip-coating the substrate into the micellar solution. EISA could be performed faster by heating the vertically oriented, dip-coated glass slide at 100 °C in air for 30 min (Scheme 1). As shown in Figure 1, the BnOH-assisted method resulted in the formation of a

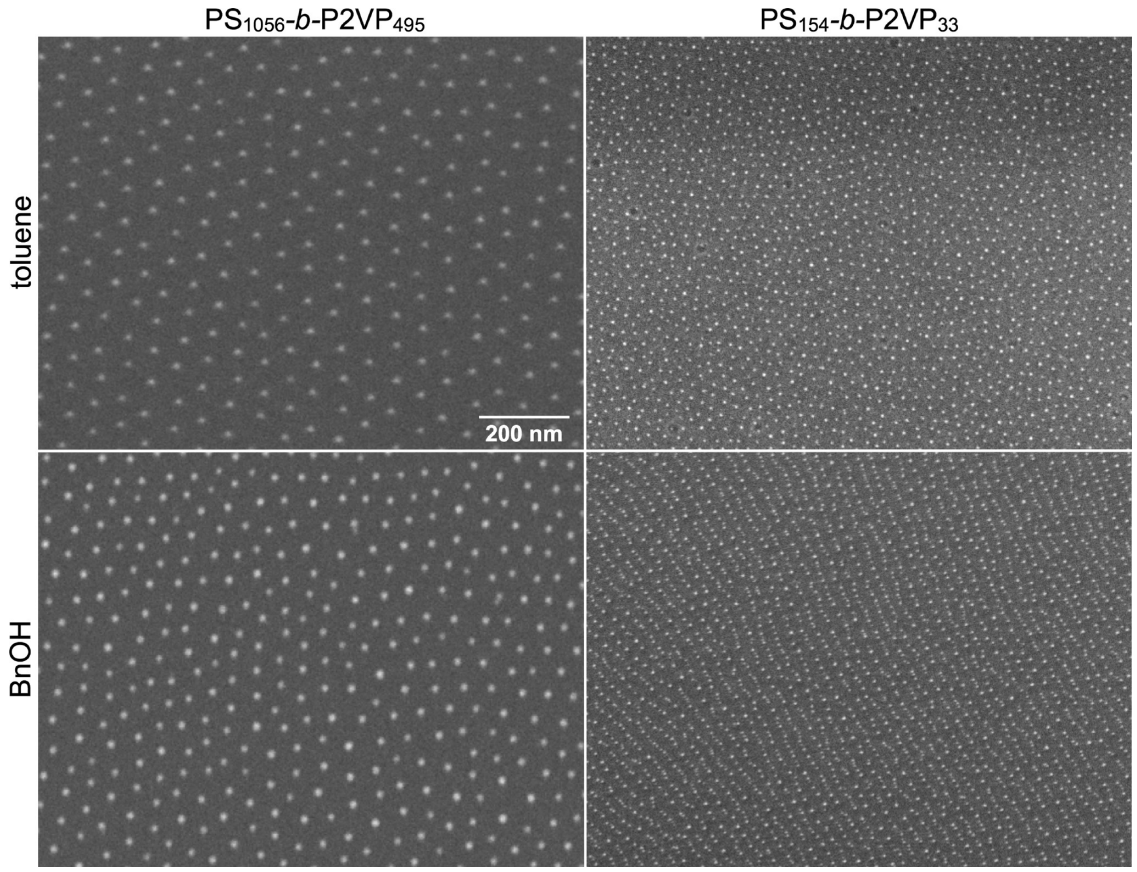

Figure 1. SEM images displaying gold nanopatterns prepared with toluene- and BnOH-assisted micellar lithographies by using two different dBCPs: PS_{1056}-*b*-$P2VP_{495}$ and PS_{154}-*b*-$P2VP_{33}$.

quasi-hexagonally organized gold nanoarray of particles of 11 ± 1 nm in diameter separated by 57 ± 6 nm (Figure 1 and S1a). In comparison, 8 ± 1 nm dots with an interspacing of 67 ± 5 nm were obtained with toluene. To learn more about micellization, we performed dynamic light scattering (DLS) measurements in both solvents, with and without gold salt. In the case of toluene, the average hydrodynamic diameter of the micelles is about 52 nm before and 69 nm after the addition of $HAuCl_4$. With BnOH, dBCP molecules do not self-assemble, as a diameter of less than 10 nm is measured. The formation of micelles with a diameter of 57 nm can be observed only in the presence of $HAuCl_4$. Schanze and colleagues reported that micellization can be induced by metal salts and used to confine and stabilize the growth of semiconductor nanoparticles in solution.[47] However, a similar method was never adapted for BCML. Due to its hydroxyl group, BnOH is a hydrogen bond (HB) donor, which interacts with P2VP (HB acceptor) and prevents dBCPs from micellizing, in contrast to toluene (no HB). Upon adding $HAuCl_4$, the P2VP block gets protonated, interacts electrostatically with $[AuCl_4]^-$, and leads to micellization. The smaller separation distance and larger gold particle diameter obtained with BnOH in comparison to toluene indicate that BnOH decreases the PS solubility and increases the compact nature of the outer micellar shell. As there is one $[AuCl_4]^-$ for two P2VP groups (*cf*. Experimental Methods), the presence of BnOH in the micellar core induces P2VP swelling and facilitates uptake of gold.

Both solvents were also used in testing other dBCPs including PS_{501}-*b*-$P2VP_{323}$ and PS_{240}-*b*-$P2VP_{143}$, and quasi-hexagonally ordered nanopatterns were obtained routinely (Figure S2). The one exception is PS_{154}-*b*-$P2VP_{33}$ in BnOH. In this case, one-dimensional patterns made of particles of 3 ± 1 nm in diameter and laterally separated by 27 ± 5 nm were observed with BnOH. In contrast, hexagonally organized 3 ± 1 nm dots with a 27 ± 5 nm spacing were generated with toluene (Figures 1 and S1b). It is interesting to note that the particle separation distance and diameter remain similar in both solvents with such a low molecular weight polymer. Therefore, it is tempting to speculate that the higher N_{PS}/N_{P2VP} ratio of PS_{154}-*b*-$P2VP_{33}$ in comparison to the other dBCPs (Table S1), together with the higher solvation of P2VP by BnOH, might represent two favorable factors responsible for the expansion of the micelle core and for loosening the corona density to form cylindrical micelles in contrast to spherical micelles obtained in toluene.[48]

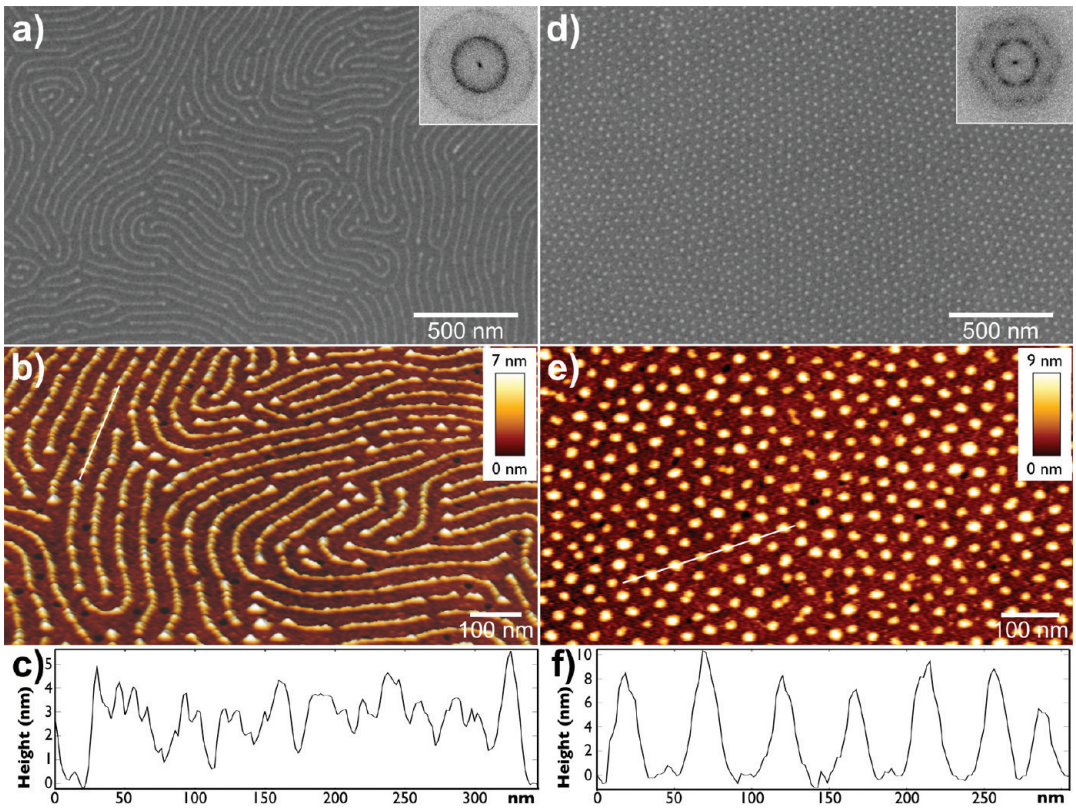

Figure 2. SEM images, scanning force micrographs, and plots of height profiles of titanium dioxide nanopatterns prepared with PS846-*b*-P2VP171 in BnOH at two different aging time points: (a, b, c) after 4 weeks and (d, e, f) after 7 weeks. Insets in (a) and (d) correspond to the power spectra of the SEM images.

Although the applicability of BnOH as a new solvent for BCML proved to be an interesting alternative to generate quasi-ordered gold nanoarrays, this method could not be extended to other systems such as titanium dioxide. That is, replacing $HAuCl_4$ with titanium tetrachloride ($TiCl_4$) did not lead to the formation of TiO_2 arrays. In contrast to sol–gel processes and chemical vapor deposition, the binding affinity of $TiCl_4$ or other titanium–BnOH complexes to the P2VP block might be too weak in solution to allow micellization. Therefore, the use of TiO_2 nanoparticles instead of molecular precursors could be helpful in increasing their affinity with P2VP.[49]

Combining Diblock Copolymer Micellar Lithography with the "Benzyl Alcohol Route" Depends on Solution Aging and the Relative Lengths of Each Polymer Block. In the field of metal oxide nanoparticle synthesis, aqueous sol–gel routes present difficulties in controlling reaction parameters (pH, hydrolysis, condensation rates of metal precursors) and particle crystallization at high temperatures.[50] A well-recognized alternative, the nonaqueous sol–gel process is based on a simpler approach that requires the solvent to act as a monodentate ligand that tailors nanoparticle features without the need for additional molecules.[51] For instance, the reaction of BnOH with different transition metal precursors such as chlorides, alkoxides, or acetylacetonates proved to be a versatile pathway to synthesize metal oxide nanoparticles with a large variety of compositions and shapes.[8,52] In the case of TiO_2, the synthesis of anatase crystals of about 4 nm in diameter has been achieved by reacting $TiCl_4$ with BnOH at 40 °C in air.[53] Although BnOH acts as a ligand to confine the growth of TiO_2 at the nanoscale, it also desorbs over time from the nanoparticle surface, leading to aggregation *via* oriented attachment.[54] To avoid this problem, it is possible to use ligands that bind to the particle surface with a stronger affinity than BnOH.[55] Because TiO_2 nanoparticles can be HB donors due to the presence of hydroxyl groups on their surface, P2VP could be used as a binding molecule[49] and PS-*b*-P2VP as an assembling agent. Since synthesis and assembly of nanoscale metal oxide systems are generally difficult to control simultaneously in a one-step approach,[6,56–58] we tested the combination of the "benzyl alcohol route" with micellar nanolithography.

In these experiments, $TiCl_4$ was first dissolved in BnOH under nitrogen and then heated at 70 °C for 5 min, which gave rise to a transparent solution stable for months. In contrast to BnOH, $TiCl_4$ was instantly solubilized in toluene but started precipitating after a few days, making this solvent unusable. PS_{1056}-*b*-$P2VP_{495}$ was then added to the BnOH solution, and the final mixture stirred for one day prior to coating. As mentioned previously, no nanostructures were observed upon dip-coating. To induce TiO_2 nanoparticle

formation, the solution was heated at 70 °C for five days. This protocol, however, did not lead to the formation of a TiO_2 nanoarray. Instead, stirring the final mixture for four additional weeks at room temperature enabled a compact layer of nanoparticles to form, probably resulting from a parallel lamellar phase, in which a less dense area made of nanowires could be observed (Figure S3). To study the influence of the dBCP composition on the final nanostructures, PS_{240}-*b*-$P2VP_{143}$, PS_{501}-*b*-$P2VP_{323}$, and PS_{2074}-*b*-$P2VP_{571}$ were tested while keeping the loading parameter equal to 0.5, as detailed in the Experimental Section. Interestingly, dBCPs with higher molecular weight and N_{PS}/N_{P2VP} ratio generated nanostructures that were less dense and more elongated (Figure S3). Although the preparation of ordered nanoarrays was not achieved with this set of dBCPs, the presence of nanoparticles was always observed despite the dilute experimental conditions, *i.e.*, using 30 times less titanium precursor in comparison to the protocol of Niederberger *et al.*[53] Ultimately, the use of polymers with a N_{PS}/N_{P2VP} ratio larger than 5 resulted in the formation of either hexagonally organized nanoparticles or parallel nanowires. Quasi-hexagonally ordered dots of 12 ± 1 nm in diameter displaying an average separation distance of 44 ± 4 nm were obtained with PS_{873}-*b*-$P2VP_{95}$ (Figure S4c,d), whereas wires with a width of 15 ± 1 nm and a lateral spacing of 50 ± 4 nm were first observed with PS_{846}-*b*-$P2VP_{171}$ (Figures 2a and S5a). Surprisingly, a morphological evolution of the nanostructures occurred upon stirring the PS_{846}-*b*-$P2VP_{171}$-containing solution for three more weeks, leading to the formation of a quasi-hexagonal array of 13 ± 2 nm particles with a spacing of 43 ± 4 nm (Figures 2d and S5b). To qualitatively characterize the lateral ordering of the different nanopatterns, power spectra of the SEM images were generated. As shown by the multiplication of the concentric rings and hexagonally distributed dots (insets, Figure 2a and d), both types of nanostructures exhibit a regular spacing and a good lateral ordering. A similar structural change was also obtained using a polymer like PS_{1776}-*b*-$P2VP_{304}$ with a molecular weight 5 times larger and a N_{PS}/P_{2VP} ratio of 5.8 (*cf.* Figure S4e,f). However, this morphological evolution did not occur with a one-year-old bottle of anhydrous benzyl alcohol or with regular benzyl alcohol, suggesting that the water content in this system is critical to control the shape transition from cylindrical to spherical. It might be that humidity conditions within the vial may change over time by simply opening it for dip-coating. As water interacts with P2VP *via* HB, the subsequent lower amount of BnOH in the vicinity of P2VP might be responsible in forming more stable spherical micelles with a smaller core, which self-assemble into a hexagonal array instead of aggregating into parallel nanowires (Figure 2). This effect is further supported by PS_{873}-*b*-$P2VP_{95}$, which did not undergo any morphological evolution due to its smaller core in comparison to PS_{846}-*b*-$P2VP_{171}$ (Figure S4c,d). Despite the low boiling point of water in comparison to BnOH, the formation of quasi-hexagonally ordered TiO_2 nanoarrays was possible by performing EISA at 100 °C and room temperature with the difference that particles were more laterally separated in the latter case (Figure S4a,b). As other groups observed the opposite morphological transition by increasing the concentration of titanium precursor,[48,59] we prepared a solution containing three times more $TiCl_4$, which led us to observe arrays of parallel TiO_2 nanowires even after 10 weeks of aging (Figure S6).

Topographic information from surfaces decorated with parallel nanowires and quasi-hexagonally ordered nanodots was obtained by atomic force microscopy (AFM, Figure 2.b,c and e,f). We observed periodic patterns across both types of nanostructures similar to the SEM images. The structures exhibit some flattening with a width-to-height ratio equal to 1.5 for the dots and 3.5 for the wires. However, despite the uniform nanowire width observed by SEM, the AFM scan shows continuous strings of connected nanoparticles along several micrometers (Figure 2b). These necklace structures exhibit periodic variations in topography every 10 nm along the wire, a height ranging from 3 to 5 nm, and a width between 12 and 15 nm (Figure 2c). These results suggest that the anisotropic flattening and aggregation of spherical micelles are necessary to form a cylindrical phase. Moreover, structural defects made of single dots of 9 nm in height can be found isolated or connected to some of the nanowire extremities. Because the average *z* value of the quasi-hexagonal nanoarrays is also about 9 nm (Figure 2f), these defects suggest the coexistence of both phases on the same substrate. Similar observations have also been described by Horvat *et al.*[60]

To further characterize the micelle features, we performed DLS measurements on the (BnOH−$TiCl_4$−PS_{846}-*b*-$P2VP_{171}$) solution at each step of the preparation procedure. Interestingly, only entities smaller than 10 nm in diameter could be detected, suggesting that both micellization and EISA occur simultaneously during BnOH evaporation (Figure S7b). Ozin and co-workers reported a similar mechanism in the case of TiO_2 mesoporous films synthesized in the presence of Pluronic P123.[61,62] Moreover, the growth of TiO_2 appeared to be more controlled in the presence of polymers than without, as we failed to detect large aggregates after one month of aging (Figure S7). Therefore, one can assign the dBCP role to be that of both a ligand and an assembling agent during the aging step and the evaporation of BnOH, respectively.

To verify the chemical composition of these surfaces, we performed X-ray photoelectron spectroscopy (XPS). Figure 3a shows the Ti2p regions of the X-ray photoelectron spectra of a micellar monolayer before

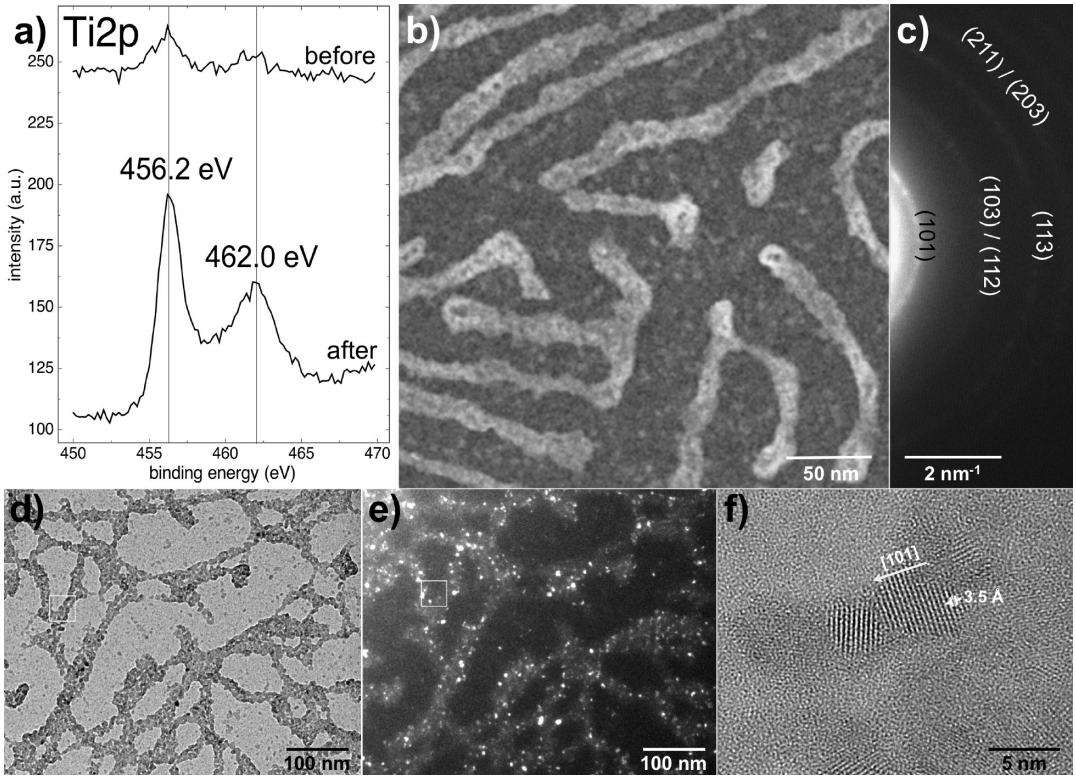

Figure 3. Structural characterization of titanium oxide nanostructures prepared with a solution of BnOH−$TiCl_4$−PS846-*b*-P2VP171 after oxygen plasma treatment. (a) Ti2p XPS spectrum of a TiO_2 nanopattern deposited onto a silicon wafer before and after plasma treatment. (b) STEM dark-field micrograph and (c) SAED pattern of TiO_2 nanostructures upon drying a 2 μL drop of the same solution at 100 °C onto a copper EM grid covered with a SiO_x membrane. (d) TEM bright-field, (e) TEM dark-field, and (f) high-resolution TEM micrographs of TiO_2 nanostructures obtained with a 4-month-old BnOH−$TiCl_4$−PS846-*b*-P2VP171 solution.

and after exposure to oxygen plasma. The spectrum clearly reveals that plasma treatment leads to the characteristic doublet $Ti2p_{3/2}$−$Ti2p_{1/2}$ at 456.2 and 462.0 eV, respectively,[41] with a binding energy difference, $\Delta E_b = E_b(Ti2p_{1/2}) - E_b(Ti2p_{3/2})$, of about 5.8 eV, which is in good agreement with the valence state of Ti^{4+} in TiO_2.[63] This doublet could also be observed with a weaker intensity before plasma exposure, suggesting the embedding of preformed TiO_2 nanoparticles in the micellar monolayer. It is important to note that some Ti^{3+} species might also be formed due to the presence of structural defects on the nanoparticle surface.[41]

To gain more insight into the formation mechanism of these TiO_2-based nanopatterns, we prepared a specimen for transmission electronic microscopy (TEM) upon drop-casting 2 μL of BnOH−$TiCl_4$−PS_{846}-*b*-$P2VP_{171}$ solution onto a copper grid covered with a SiO_x membrane. Figure 3b displays elongated nanostructures of 15 nm in width composed of individual grains of about 3−4 nm in diameter. These grains exhibit a more compact nature as compared to other reports describing the preparation of nanopatterns *via* the assembly of nano-objects directed by templating molecules.[24−26,43−45,59] Selected area electron diffraction (SAED) indicates the polycrystalline nature of the nanostructures randomly oriented on the SiO_x membrane (Figure 3c). The Debye−Scherrer inner ring shows a lattice plane spacing of around 3.5 Å, which corresponds to the lattice spacing for the (101) plane of anatase, thus excluding the presence of the rutile phase. Since pure anatase was always identified by reacting $TiCl_4$ with BnOH,[53−55,64] we assume that brookite could not be synthesized with the present route. By using the "benzyl alcohol route" these 3−4 nm building blocks are obviously confined within the micelle core during micellization and rarely localized in between the nanopattern. Interestingly, by using the same solution after four months of stirring at room temperature, elongated structures made of larger grains of about 5 nm were obtained, suggesting that TiO_2 continues growing slowly after the 5-day heating step. Upon aging the solution for several weeks, the nanoparticles may reach the necessary size, concentration, or surface composition that enables them to induce micellization prior to their self-assembly during solvent evaporation. In addition, the larger grains of this specimen appear with bright contrast at different dark-field conditions due to their random crystal orientation (Figure 3e). In the high-resolution TEM micrograph, grains with suitable orientation show anatase (101) lattice fringes of *ca.* 3.5 Å (Figure 3f). The random nanocrystal orientation indicates that each grain was possibly surrounded by vinylpyridine groups before

plasma treatment, which did not allow the formation of monocrystalline nanostructures *via* oriented attachment.[54] The experimental procedures and the formation mechanism of this approach are summarized in Scheme 2.

Simple Fabrication of Gold–Titanium Dioxide Binary Nanoarrays. From an application standpoint, nanopatterned substrates represent not only a potentially important platform for a number of different technological fields[13,14] but also a starting material for the construction of more sophisticated nanostructures.[65–67] The preparation of surfaces made of two different ordered nanopatterns is interesting for tailoring the physicochemical properties of such interfaces. Only a few groups have reported straightforward synthetic strategies. These include the design of Au-γFe_2O_3 *via* micellar nanolithography and postdeposition of alkyl-coated gold colloids,[65] Au-PtO/PtO_x *via* lithography using a mixture of loaded-micellar solutions,[68] CdSe@ZnS-γFe_2O_3 *via* the deposition of dispersed nanoparticles onto thin polymer films reconstructed by chemical epitaxy,[45] and CdS-TiO_2 with the help of dispersed micelles made of a TiO_2 core and a shell decorated with quantum dots.[69] However, the organization of such monolayered materials over a large scale remains a difficult task due to the imprecise positioning of the second nanoarray that often exhibits an uncontrolled particle distribution and density.

In contrast to the previous approaches, for these experiments we employed a simple two-step dip-coating procedure by processing the same substrate twice. Figure 4 displays the final nanostructures resulting from the deposition of various TiO_2 nanoarrays on preformed gold nanopatterns. Surprisingly, the nanowire separation distance and the quasi-hexagonal organization of the nanoparticles were not disturbed by the presence of the gold patterns (Figures 4a and b, S8, and S9). Despite their different periodicities, *i.e.*, 49 nm for TiO_2 and 65 nm for gold, the placement of quasi-hexagonally organized TiO_2 nanodots occurred between and in close contact to gold particles, but rarely on top of them (Figure S9a,b). Moreover, the same observation was done on a nanopattern with a commensurate configuration, *i.e.*, 49 nm separation distance for TiO_2 and 96 nm for gold (Figure 4b). For clarity, hexagonal overlays were drawn on the SEM images in order to distinguish the position of both quasi-ordered structures (Figure S9). Because TiO_2 is arranged independently from the gold nanoarray, the even distribution of both materials allows the control of their density in a precise way. In contrast to 8 nm gold dots, particles of 25 nm in diameter could disturb the order of TiO_2 where local organization was sometimes induced, as hexagonal rings around enlarged gold dots could be observed (Figure 4c). In comparison to the structures reported by Bita *et al.* (Figure 4c, inset),[70] the lack of TiO_2 order induced by graphoepitaxy might come from the presence of defects in the gold nanoarrays, which are difficult to avoid with a spacing larger than 100 nm and upon gold enlargement. It is important to mention that top-down approaches, like electron-beam lithography, were always utilized in reports dealing with grapho- and chemical epitaxy because of their excellent accuracy in designing 2D periodic patterned templates.[70,71]

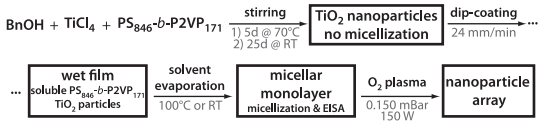

Scheme 2. Schematics depicting the experimental procedure and the formation mechanism of TiO_2 nanoarrays *via* BnOH-assisted micellar lithography.

To qualitatively characterize the lateral ordering of the binary nanoarrays, power spectra of the SEM images were generated. As displayed in Figure S10, the six

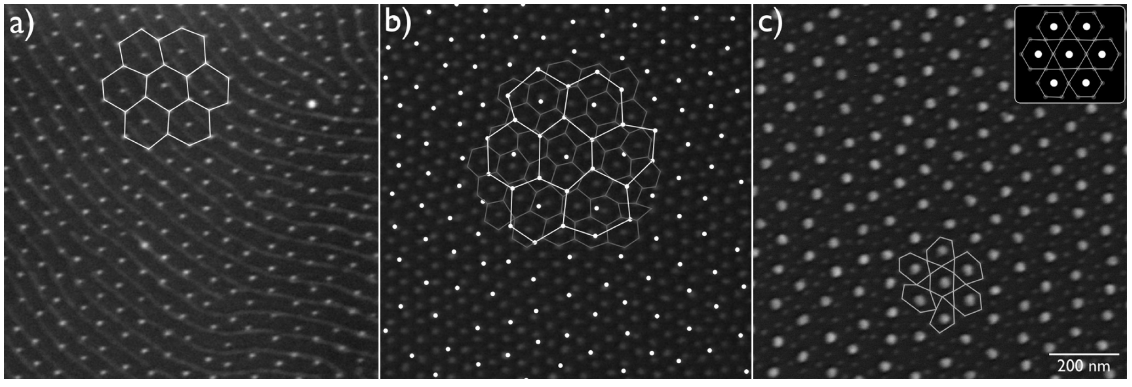

Figure 4. SEM images of Au-TiO_2 binary nanoarrays resulting from the deposition of various titanium dioxide nanostructures onto different quasi-hexagonal gold nanopatterns. (a) TiO_2 aligned nanowires with a spacing of 55 nm deposited onto a gold nanopattern with a separation distance of 71 nm. (b) TiO_2 array with a 49 nm spacing deposited onto a gold nanopattern with a 96 nm separation distance. Due to their differences in size and electrical conductivity, gold usually appears brighter. For clarity, a hexagonal overlay is drawn on the gold nanoarray. (c) The same Au-TiO_2 binary array as in (b), with the difference that gold dots were enlarged from 8 nm to 25 nm in diameter upon electroless deposition before coating the substrate with TiO_2. Hexagonal overlays display a few examples of locally organized TiO_2 induced by the gold nanoarray. Inset shows a perfectly organized binary nanoarray, as reported by Bita *et al.*

spots in the central part of the power spectrum surrounded by a second hexagonal ring made of broader spots are characteristic for the quasi-organization of gold and titania nanoarrays when prepared individually. Interestingly, the power spectrum of Au-TiO_2 binary nanoarrays exhibits features of both materials, which further suggests the ordering conservation of both structures. However, we found that switching the dip-coating sequence influences the final structure of the binary nanoarrays (Figure S10). We observed that more than 70% of gold nanodots position in contact with TiO_2 particles when gold nanopatterns are deposited onto TiO_2 nanoarrays. This effect slightly disturbs the organization of gold, as shown by the power spectrum (Figure S10). In the opposite case, as TiO_2 dots position independently on the gold nanoarray, only 35% of particles are in contact with each other. Although the PS outer shell of the micelles, upon interfacing either gold or titania nanoarrays during the second dip-coating step, is obviously more attracted by single TiO_2 nanodots, this observation could not be fully understood.

CONCLUSION

In the present study, we report a straightforward version of block copolymer micellar lithography applicable to gold and titanium dioxide by using BnOH as a solvent. In comparison to toluene, BnOH leads to the formation of various gold nanopatterns *via* salt-induced micellization with PS-*b*-P2VP. In the case of titania, the data validate the concept of integrating the "benzyl alcohol route" with micellar nanolithography, which was found to depend mainly on the aging of the BnOH−$TiCl_4$−PS_{846}-*b*-$P2VP_{171}$ solution to form TiO_2 building blocks of 3−4 nm in diameter and the relative lengths of the polymer blocks, *i.e.*, N_{PS}/N_{P2VP} ratio. The *in situ* growth of TiO_2 in BnOH and its subsequent assembly during EISA proved to be effective in the preparation of 2D-organized isotropic and anisotropic nanostructures. Despite the long aging step required to grow TiO_2 particles sufficiently, this method remains direct, without the need of other polluting solvents and without additional steps such as solvent annealing, postincorporation of metallic precursors, or prefunctionalization of presynthesized nanoparticles. The prepared solutions can be used for several months under ambient conditions when stored at 4 °C to stop the particle growth. In addition, this versatile route enables the design of uniform Au-TiO_2 binary nanoarrays of various morphologies with a precise particle density.

The reported approach could be generalized to many other hybrid and inorganic systems, which are already available *via* the BnOH route. Moreover, since it is possible to tailor a variety of properties characteristic of nanomaterials, the directed assembly of binary or ternary systems would make them ideal candidates to design the next generations of multifunctional interfaces. Potential opportunities include etching masks to structure substrates with different depths and morphologies, catalysts to grow several types of anisotropic nanostructures, and scaffolds for immobilizing two different types of molecules by taking advantage of the distinct chemistries for surface modification of metals and metal oxides.

EXPERIMENTAL METHODS

In a typical synthesis, polystyrene(*x*)-*block*-poly(2-vinylpyridine)(*y*) (PS_x-*b*-$P2VP_y$, where *x* and *y* represent the number of monomer units) from Polymer Source Inc. was dissolved at room temperature in anhydrous toluene (Sigma-Aldrich) or anhydrous benzyl alcohol (BnOH, Sigma-Aldrich) and stirred for 1 day. The quantity of inorganic precursor was calculated relative to the number of P2VP units (N_{P2VP}) and defined as the loading parameter (*L*). *L* was kept constant in all experiments, equal to 0.5, *i.e.*, 1 molecule of $HAuCl_4$ or $TiCl_4$ for 2 P2VP monomers. Hydrogen tetrachloroaurate(III) trihydrate ($HAuCl_4 \cdot 3H_2O$, Sigma-Aldrich) was added to the dBCP solution and stirred for 1 day in a sealed glass vessel. For the preparation of titanium dioxide solutions, 2.2 μL of titanium tetrachloride ($TiCl_4$, Sigma-Aldrich) was dissolved under nitrogen in 5 mL of BnOH. The solution was heated for 5 min at 70 °C in an oil bath for better dissolution. Upon stirring at room temperature for 3 h, 25 mg of PS_x-*b*-$P2VP_y$ was added to the solution and stirred 15 h at room temperature. In order to induce TiO_2 particle formation, the solution was stirred at 70 °C for 5 days. After aging the solution for several weeks at room temperature, a yellow solution was obtained. Glass coverslips (Carl Roth) were cleaned in a piranha solution for at least 5 h and were extensively rinsed with Milli-Q water and dried under a stream of nitrogen. Micellar monolayers were prepared by dip-coating a glass coverslip into the previously prepared solutions with a constant velocity equal to 24 mm · min^{-1}. In the case of BnOH, the samples were dried in an oven at 100 °C for 30 min. Finally, to remove the organic template and to form inorganic nanoparticles, the dip-coated glass slides were exposed to oxygen plasma (150 W, 0.15 mbar, 45 min, PVA TEPLA 100 Plasma System). For the preparation of binary nanopatterns, gold nanoarrays with the desired spacing were simply dip-coated into a BnOH−$TiCl_4$−PS_x-*b*-$P2VP_y$ solution. The enlargement of gold nanodots was perform according to the procedure reported by Lohmueller *et al.*[72]

Scanning electron measurements were performed with a Dual Beam (FIB/SEM) instrument (Quanta 3D FEG, FEI, Hillsboro). Power spectra, the square of the Fourier transform of a SEM image, were performed with Scion Image software. Atomic force microscopy was performed with a "Nano Wizard I" AFM (JPK Instruments AG) mounted on an optical microscope (Zeiss Axiovert 200). Atomic force micrographs were obtained in air using intermittent contact mode with a single-crystal diamond cantilever with a radius of curvature of 7 nm and antiflattening properties (μMasch, SCD18). X-ray photoelectron spectroscopy was performed with a Leybold MAX 200 photoelectron spectrometer equipped with an Al Kα radiation source (1486.6 eV) operated at 200 W. Emitted photoelectrons were detected by a multichannel detector at a pass energy of 96 eV for the survey spectra and of 48 eV for narrow-scanned spectra, respectively, and a takeoff angle of 90° relative to the surface. A Precision

Detector DD2000 DLS^{PLUS} laser scattering system equipped with a PDDLS/CoolBatch901 was used to perform dynamic light scattering experiments. The hydrodynamic radius of the micelles was measured with the Precision Deconvolve software. Transmission electron microscopy was done at 200 kV on a JEOL-2010F field-emission instrument with an ultra-high-resolution pole piece. The microscope was used for selected area electron diffraction and in different contrast modes: scanning transmission electron microscope (STEM) high-angle annular dark-field (HAADF), TEM bright-field, TEM dark-field, and phase contrast (*i.e.*, high-resolution TEM (HRTEM)).

Acknowledgment. We thank R. Fässler and B. Dunn for support and careful reading of the manuscript, and A. Rigort for his continuous help with electronic microscopy. The 7th Framework Program of the European Community (FP7) through the Marie Curie Action for career development (IEF—"Multi-PGNAs") and the Max Planck Society financially supported this work.

Supporting Information Available: Tables summarizing information related to the block copolymers and the prepared nanoarrays; additional low- and high-magnification SEM images; DLS data; and power spectra of SEM images. This material is available free of charge *via* the Internet at http://pubs.acs.org.

REFERENCES AND NOTES

1. Alivisatos, A. Perspectives on the Physical Chemistry of Semiconductor Nanocrystals. *J. Phys. Chem.* **1996**, *100*, 13226–13239.
2. El-Sayed, M. Small is Different: Shape-, Size-, and Composition-Dependent Properties of Some Colloidal Semiconductor Nanocrystals. *Acc. Chem. Res.* **2004**, *37*, 326–333.
3. Sanchez, C.; Soler-Illia, G.; Ribot, F.; Lalot, T.; Mayer, C.; Cabuil, V. Designed Hybrid Organic-Inorganic Nanocomposites from Functional Nanobuilding Blocks. *Chem. Mater.* **2001**, *13*, 3061–3083.
4. Scher, E.; Manna, L.; Alivisatos, A. Shape Control and Applications of Nanocrystals. *Philos. Trans. R. Soc A* **2003**, *361*, 241–255.
5. Wang, Y.; Herron, N. Nanometer-Sized Semiconductor Clusters - Materials Synthesis, Quantum Size Effects, and Photophysical Properties. *J. Phys. Chem.* **1991**, *95*, 525–532.
6. Antonietti, M.; Niederberger, M.; Smarsly, B. Self-Assembly in Inorganic and Hybrid Systems: Beyond the Molecular Scale. *Dalton Trans.* **2008**, 18–24.
7. Antonietti, M.; Ozin, G. Promises and Problems of Mesoscale Materials Chemistry or Why Meso? *Chem.—Eur. J.* **2004**, *10*, 29–41.
8. Niederberger, M. Nonaqueous Sol-Gel Routes to Metal Oxide Nanoparticles. *Acc. Chem. Res.* **2007**, *40*, 793–800.
9. Shevchenko, E.; Talapin, D.; Kotov, N.; O'Brien, S.; Murray, C. Structural Diversity in Binary Nanoparticle Superlattices. *Nature* **2006**, *439*, 55–59.
10. Talapin, D. V.; Shevchenko, E. V.; Bodnarchuk, M. I.; Ye, X.; Chen, J.; Murray, C. B. Quasi-Crystalline Order in Self-Assembled Binary Nanoparticle Superlattices. *Nature* **2009**, *461*, 964–967.
11. Smarsly, B.; Antonietti, M. Block Copolymer Assemblies As Templates for the Generation of Mesoporous Inorganic Materials and Crystalline Films. *Eur. J. Inorg. Chem.* **2006**, 1111–1119.
12. Zhang, G.; Wang, D. Colloidal Lithography - The Art of Nanochemical Patterning. *Chem.—Asian J* **2009**, *4*, 236–245.
13. Bang, J.; Jeong, U.; Ryu, D. Y.; Russell, T. P.; Hawker, C. J. Block Copolymer Nanolithography: Translation of Molecular Level Control to Nanoscale Patterns. *Adv. Mater.* **2009**, *21*, 4769–4792.
14. Darling, S. B. Directing the Self-Assembly of Block Copolymers. *Prog. Polym. Sci.* **2007**, *32*, 1152–1204.
15. Kim, H.-C.; Park, S.-M.; Hinsberg, W. D. Block Copolymer Based Nanostructures: Materials, Processes, and Applications to Electronics. *Chem. Rev.* **2010**, *110*, 146–177.
16. Stoykovich, M. P.; Nealey, P. F. Block Copolymers and Conventional Lithography. *Mater. Today* **2006**, *9*, 20–29.
17. Forster, S. Amphiphilic Block Copolymers for Templating Applications. *Top. Curr. Chem.* **2003**, *226*, 1–28.
18. Brinker, C.; Lu, Y.; Sellinger, A.; Fan, H., Evaporation-Induced Self-Assembly: Nanostructures Made Easy. *Adv. Mater.* **1999**, *11*, 579.
19. Li, M.; Ober, C. K. Block Copolymer Patterns and Templates. *Mater. Today* **2006**, *9*, 30–39.
20. Park, M.; Harrison, C.; Chaikin, P.; Register, R.; Adamson, D. Block Copolymer Lithography: Periodic Arrays of Similar to 10^{11} Holes in 1 Square Centimeter. *Science* **1997**, *276*, 1401–1404.
21. Brezesinski, T.; Groenewolt, M.; Gibaud, A.; Pinna, N.; Antonietti, M.; Smarsly, B. M. Evaporation-Induced Self-Assembly (EISA) at its Limit: Ultrathin, Crystalline Patterns by Templating of Micellar Monolayers. *Adv. Mater.* **2006**, *18*, 2260–2263.
22. Chai, J.; Buriak, J. M. Using Cylindrical Domains of Block Copolymers to Self-Assemble and Align Metallic Nanowires. *ACS Nano* **2008**, *2*, 489–501.
23. Glass, R.; Arnold, M.; Blummel, J.; Kuller, A.; Moller, M.; Spatz, J. Micro-Nanostructured Interfaces Fabricated by the Use of Inorganic Block Copolymer Micellar Monolayers As Negative Resist for Electron-Beam Lithography. *Adv. Funct. Mater.* **2003**, *13*, 569–575.
24. Fahmi, A.; Pietsch, T.; Mendoza, C.; Cheval, N. Functional Hybrid Materials. *Mater. Today* **2009**, *12*, 44–50.
25. Haryono, A.; Binder, W. Controlled Arrangement of Nanoparticle Arrays in Block-Copolymer Domains. *Small* **2006**, *2*, 600–611.
26. Nandan, B.; Gowd, E. B.; Bigall, N. C.; Eychmueller, A.; Formanek, P.; Simon, P.; Stamm, M. Arrays of Inorganic Nanodots and Nanowires Using Nanotemplates Based on Switchable Block Copolymer Supramolecular Assemblies. *Adv. Funct. Mater.* **2009**, *19*, 2805–2811.
27. Kastle, G.; Boyen, H.; Weigl, F.; Lengl, G.; Herzog, T.; Ziemann, P.; Riethmuller, S.; Mayer, O.; Hartmann, C.; Spatz, J.; Moller, M.; Ozawa, M.; Banhart, F.; Garnier, M.; Oelhafen, P. Micellar Nanoreactors - Preparation and Characterization of Hexagonally Ordered Arrays of Metallic Nanodots. *Adv. Funct. Mater.* **2003**, *13*, 853–861.
28. Krishnamoorthy, S.; Hinderling, C.; Heinzelmann, H. Nanoscale Patterning with Block Copolymers. *Mater. Today* **2006**, *9*, 40–47.
29. Yun, H.-S.; Zhou, H.; Honma, I. Preparation of Self-Standing, Submillimeter-Thick Porous Titania Films with Anatase Nanocrystallites Using Evaporation-Induced Self-Assembly. *J. Inorg. Organomet. Polym.* **2006**, *16*, 169–173.
30. Sokolov, S.; Ortel, E.; Kraehnert, R. Mesoporous Titania Films with Adjustable Pore Size Coated on Stainless Steel Substrates. *Mater. Res. Bull.* **2009**, *44*, 2222–2227.
31. Strandwitz, N. C.; Nonoguchi, Y.; Boettcher, S. W.; Stucky, G. D. *In Situ* Photopolymerization of Pyrrole in Mesoporous TiO_2. *Langmuir* **2010**, *26*, 5319–5322.
32. Kim, Y. J.; Lee, Y. H.; Lee, M. H.; Kim, H. J.; Pan, J. H.; Lim, G. I.; Choi, Y. S.; Kim, K.; Park, N.-G.; Lee, C.; *et al.* Formation of Efficient Dye-Sensitized Solar Cells by Introducing an Interfacial Layer of Long-Range Ordered Mesoporous TiO_2 Thin Film. *Langmuir* **2008**, *24*, 13225–13230.
33. Zhang, Y.; Xie, Z.; Wang, J. Supramolecular-Templated Thick Mesoporous Titania Films for Dye-Sensitized Solar Cells: Effect of Morphology on Performance. *ACS Appl. Mater. Interfaces* **2009**, *1*, 2789–2795.
34. Dambournet, D.; Belharouak, I.; Amine, K. Tailored Preparation Methods of TiO_2 Anatase, Rutile, Brookite: Mechanism of Formation and Electrochemical Properties. *Chem. Mater.* **2010**, *22*, 1173–1179.
35. Wang, J.; Polleux, J.; Lim, J.; Dunn, B. Pseudocapacitive Contributions to Electrochemical Energy Storage in TiO_2 (Anatase) Nanoparticles. *J. Phys. Chem. C* **2007**, *111*, 14925–14931.
36. Wang, Z.; Kawauchi, H.; Kashima, T.; Arakawa, H. Significant Influence of TiO_2 Photoelectrode Morphology on the Energy Conversion Efficiency of N719 Dye-Sensitized Solar Cell. *Coord. Chem. Rev.* **2004**, *248*, 1381–1389.
37. Yan, M.; Chen, F.; Zhang, J.; Anpo, M. Preparation of Controllable Crystalline Titania and Study on the Photocatalytic Properties. *J. Phys. Chem. B* **2005**, *109*, 8673–8678.

38. Cheng, Y.; Gutmann, J. Morphology Phase Diagram of Ultrathin Anatase TiO_2 Films Templated by a Single PS-b-PEO Block Copolymer. *J. Am. Chem. Soc.* **2006**, *128*, 4658–4674.
39. Kuemmel, M.; Allouche, J.; Nicole, L.; Boissiere, C.; Laberty, C.; Amenitsch, H.; Sanchez, C.; Grosso, D. A Chemical Solution Deposition Route to Nanopatterned Inorganic Material Surfaces. *Chem. Mater.* **2007**, *19*, 3717–3725.
40. Sun, Z.; Kim, D.; Wolkenhauer, M.; Bumbu, G.; Knoll, W.; Gutmann, J. Synthesis and Photoluminescence of Titania Nanoparticle Arrays Templated by Block-Copolymer Thin Films. *ChemPhysChem* **2006**, *7*, 370–378.
41. Yuwono, A. H.; Zhang, Y.; Wang, J.; Zhang, X. H.; Fan, H.; Ji, W. Diblock Copolymer Templated Nanohybrid Thin Films of Highly Ordered TiO_2 Nanoparticle Arrays in PMMA Matrix. *Chem. Mater.* **2006**, *18*, 5876–5889.
42. Li, X.; Lau, K.; Kim, D.; Knoll, W. High-Density Arrays of Titania Nanoparticles Using Monolayer Micellar Films of Diblock Copolymers As Templates. *Langmuir* **2005**, *21*, 5212–5217.
43. Weng, C.; Wei, K. Selective Distribution of Surface-Modified TiO_2 Nanoparticles in Polystyrene-b-Poly(methyl methacrylate) Diblock Copolymer. *Chem. Mater.* **2003**, *15*, 2936–2941.
44. Shenhar, R.; Jeoung, E.; Srivastava, S.; Norsten, T.; Rotello, V. Crosslinked Nanoparticle Stripes and Hexagonal Networks Obtained *via* Selective Patterning of Block Copolymer Thin Films. *Adv. Mater.* **2005**, *17*, 2206–2210.
45. Son, J. G.; Bae, W. K.; Kang, H.; Nealey, P. F.; Char, K. Placement Control of Nanomaterial Arrays on the Surface-Reconstructed Block Copolymer Thin Films. *ACS Nano* **2009**, *3*, 3927–3934.
46. Hashimoto, T.; Harada, M.; Sakamoto, N. Incorporation of Metal Nanoparticles Into Block Copolymer Nanodomains *via In Situ* Reduction of Metal Ions in Microdomain Space. *Macromolecules* **1999**, *32*, 6867–6870.
47. Zhao, H.; Douglas, E.; Harrison, B.; Schanze, K. Preparation of CdS Nanoparticles in Salt-Induced Block Copolymer Micelles. *Langmuir* **2001**, *17*, 8428–8433.
48. Song, L.; Lam, Y. M.; Boothroyd, C.; Teo, P. W. One-Step Synthesis of Titania Nanoparticles from PS-P4VP Diblock Copolymer Solution. *Nanotechnology* **2007**, *18*, 135605.
49. Malynych, S.; Luzinov, I.; Chumanov, G. Poly(vinylpyridine) As a Universal Surface Modifier for Immobilization of Nanoparticles. *J. Phys. Chem. B* **2002**, *106*, 1280–1285.
50. Matijevic, E. Preparation and Properties Of Uniform Size Colloids. *Chem. Mater.* **1993**, *5*, 412–426.
51. Garnweitner, G.; Niederberger, M. Organic Chemistry in Inorganic Nanomaterials Synthesis. *J. Mater. Chem.* **2008**, *18*, 1171–1182.
52. Niederberger, M.; Garnweitner, G. Organic Reaction Pathways in the Nonaqueous Synthesis of Metal Oxide Nanoparticles. *Chem.—Eur. J.* **2006**, *12*, 7282–7302.
53. Niederberger, M.; Bartl, M.; Stucky, G. Benzyl Alcohol and Titanium Tetrachloride - A Versatile Reaction System for the Nonaqueous and Low-Temperature Preparation of Crystalline and Luminescent Titania Nanoparticles. *Chem. Mater.* **2002**, *14*, 4364–4370.
54. Polleux, J.; Pinna, N.; Antonietti, M.; Hess, C.; Wild, U.; Schlögl, R.; Niederberger, M. Ligand Functionality As a Versatile Tool to Control the Assembly Behavior of Preformed Titania Nanocrystals. *Chem.—Eur. J.* **2005**, *11*, 3541–3551.
55. Niederberger, M.; Garnweitner, G.; Krumeich, F.; Nesper, R.; Colfen, H.; Antonietti, M. Tailoring the Surface and Solubility Properties of Nanocrystalline Titania by a Nonaqueous *In Situ* Functionalization Process. *Chem. Mater.* **2004**, *16*, 1202–1208.
56. Polleux, J.; Antonietti, M.; Niederberger, M. Ligand and Solvent Effects in the Nonaqueous Synthesis of Highly Ordered Anisotropic Tungsten Oxide Nanostructures. *J. Mater. Chem.* **2006**, *16*, 3969.
57. Polleux, J.; Gurlo, A.; Barsan, N.; Weimar, U.; Antonietti, M.; Niederberger, M. Template-Free Synthesis and Assembly of Single-Crystalline Tungsten Oxide Nanowires and their Gas-Sensing Properties. *Angew. Chem., Int. Ed.* **2006**, *45*, 261–265.
58. Pinna, N. The "Benzyl Alcohol Route": an Elegant Approach towards Organic-Inorganic Hybrid Nanomaterials. *J. Mater. Chem.* **2007**, *17*, 2769–2774.
59. Peng, J.; Mao, C.; Kim, J.; Kim, D. H. From Nanodot to Nanowire: Hybrid Au/Titania Nanoarrays by Block Copolymer Templates. *Macromol. Rapid Commun.* **2009**, *30*, 1857–1861.
60. Horvat, A.; Sevink, G. J. A.; Zvelindovsky, A. V.; Krekhov, A.; Tsarkova, L. Specific Features of Defect Structure and Dynamics in the Cylinder Phase of Block Copolymers. *ACS Nano* **2008**, *2*, 1143–1152.
61. Choi, S.; Mamak, M.; Coombs, N.; Chopra, N.; Ozin, G. Thermally Stable Two-Dimensional Hexagonal Mesoporous Nanocrystalline Anatase, Meso-nc-TiO_2: Bulk and Crack-Free Thin Film Morphologies. *Adv. Funct. Mater.* **2004**, *14*, 335–344.
62. Hung, I.-M.; Wang, Y.; Huang, C.-F.; Fan, Y.-S.; Han, Y.-J.; Peng, H.-W. Effects of Templating Surfactant Concentrations on the Mesostructure of Ordered Mesoporous Anatase TiO_2 by an Evaporation-Induced Self-Assembly Method. *J. Eur. Ceram. Soc.* **2010**, *30*, 2065–2072.
63. Pouilleau, J.; Devilliers, D.; Groult, H.; Marcus, P. Surface Study of a Titanium-Based Ceramic Electrode Material by X-ray Photoelectron Spectroscopy. *J. Mater. Sci.* **1997**, *32*, 5645–5651.
64. Polleux, J.; Pinna, N.; Antonietti, M.; Niederberger, M. Ligand-Directed Assembly of Preformed Titania Nanocrystals into Highly Anisotropic Nanostructures. *Adv. Mater.* **2004**, *16*, 436–439.
65. Sohn, B.; Choi, J.; Yoo, S.; Yun, S.; Zin, W.; Jung, J.; Kanehara, M.; Hirata, T.; Teranishi, T. Directed Self-Assembly of Two Kinds of Nanoparticles Utilizing Monolayer Films of Diblock Copolymer Micelles. *J. Am. Chem. Soc.* **2003**, *125*, 6368–6369.
66. Brezesinski, T.; Antonietti, M.; Smarsly, B. M. Self-Assembled Metal Oxide Bilayer Films with "Single-Crystalline" Overlayer Mesopore Structure. *Adv. Mater.* **2007**, *19*, 1074–1078.
67. Brezesinski, T.; Wang, J.; Tolbert, S. H.; Dunn, B. Ordered Mesoporous Alpha-MoO_3 with Iso-Oriented Nanocrystalline Walls for Thin-Film Pseudocapacitors. *Nat. Mater.* **2010**, *9*, 146–151.
68. Chang, J.-J.; Kwon, J.-H.; Yoo, S. I.; Park, C.; Sohn, B.-H. Bimodal Arrays of Two Types of Nanoparticles by Mixtures of Diblock Copolymer Micelles. *J. Mater. Chem.* **2009**, *19*, 1621–1625.
69. Kannaiyan, D.; Kim, E.; Won, N.; Kim, K. W.; Jang, Y. H.; Cha, M.-A.; Ryu, D. Y.; Kim, S.; Kim, D. H. On the Synergistic Coupling Properties of Composite CdS/TiO_2 Nanoparticle Arrays Confined in Nanopatterned Hybrid Thin Films. *J. Mater. Chem.* **2010**, *20*, 677.
70. Bita, I.; Yang, J. K. W.; Jung, Y. S.; Ross, C. A.; Thomas, E. L.; Berggren, K. K. Graphoepitaxy of Self-Assembled Block Copolymers on Two-Dimensional Periodic Patterned Templates. *Science* **2008**, *321*, 939–943.
71. Ruiz, R.; Kang, H.; Detcheverry, F. A.; Dobisz, E.; Kercher, D. S.; Albrecht, T. R.; De Pablo, J. J.; Nealey, P. F. Density Multiplication and Improved Lithography by Directed Block Copolymer Assembly. *Science* **2008**, *321*, 936–939.
72. Lohmueller, T.; Bock, E.; Spatz, J. P. Synthesis of Quasi-Hexagonal Ordered Arrays of Metallic Nanoparticles with Tuneable Particle Size. *Adv. Mater.* **2008**, *20*, 2297–2302.